ELSEVIER

Contents lists available at ScienceDirect

Journal of Molecular Graphics and Modelling

journal homepage: www.elsevier.com/locate/jmgm





A coarse-grained Molecular Dynamics study of phase behavior in Co-assembled lipomimetic oligopeptides

Srinivas Mushnoori ¹, Chien Y. Lu ¹, Kassandra Schmidt ¹, Meenakshi Dutt ¹

Department of Chemical and Biochemical Engineering, Rutgers, The State University of New Jersey, Piscataway, NJ-08854, USA

ARTICLE INFO

Keywords: Lipomimetic peptides Molecular dynamics Phase separation Coarse-grained models Martini

ABSTRACT

Multicomponent biomolecular aggregates, i.e., systems consisting of more than one type of biomolecular component co-assembling into one aggregate, provide an interesting design space for engineering unique biomaterials. In this study, we examine the co-assembly of two lipomimetic oligopeptide block copolymers selected for their lipid-like amphiphilicity and highly similar architectures into nanofibers via coarse-grained MD simulations. We focus on the behavior of these peptides due to incremental differences in size by selecting two peptides that differ in length by exactly one amino acid residue. We find that the longer peptide sequence displays greater self-association properties.

1. Introduction

The rich chemical diversity along with biocompatibility of peptide supramolecular assemblies have made them increasingly prevalent in applications related to biomedicine, energy and electronics. Pure peptide systems consisting primarily of aromatic amino acids have been reported to yield nanostructures including bilayers, fibers, nanospheres, nanotubes and vesicles [1] with potential use as drug delivery vehicles or solid-state devices. The assembly of longer aliphatic peptide sequences have been observed to form fibrillar structures and hydrogels with potential applications in therapeutics and electronics [2]. The co-assembly of distinct peptide sequences introduces an unique opportunity to increase the design space for these assemblies, thereby significantly expanding their functionality. Yet, the increase in the design space introduces the challenge of parsing a vast number of peptide sequences to obtain co-assemblies with target functionalities. This study explores the properties of aggregates emerging from the co-assembly of two lipomimetic aliphatic peptide sequences with the same amino acid residues but different polymerization of the polar residues with specific focus on the phase separation of the two peptide species.

Existing studies in the domain of co-assembly of peptide sequences include the formation of rippled beta sheets from the coassembly of L-and D- enantiomers of the same oligopeptide sequence [3]. Other studies include the formation of hydrogel and beta sheets from MAX1-azide and DMAX1-biotin co-assembly systems [4] and highly stable ribbon-like

structures in systems encompassing co-assembled peptides with lipids [5]. Furthermore, detailed reviews [6] have discussed studies on multicomponent peptide assemblies.

While experimental studies such as the ones discussed above are critically important to our understanding of co-assembled peptide systems, computational studies provide additional insight into the mechanistic aspects of assembly. Some of the computational studies that have been undertaken in this domain are: FF (Diphenylalanine) and FFF (Triphenylalanine) co-assembled structures were found to form fibers [1c], spheres and toroids, while FF and FNF alanine-Asparagine-Phenylalanine) co-assemblies were observed to form nanotubes, vesicles and lamellae [7]. In the latter study, the peptides were ultrashort with only two to three amino acid residues. Co-assembly studies on peptides that are comparable in size and structure to lipids, however, are scant. Our study aims to explore the co-assembly of lipomimetic peptides V₆K₂, an oligopeptide consisting of six Valine residues (V) and two Lysine (K) residues and V₆K₃, an oligopeptide consisting of six Valine residues and three Lysine residues. The two peptides are similar, with the exception for V₆K₃ having an additional Lysine residue over V₆K₂. Our study therefore seeks to understand the effects of incremental differences in polymerization while controlling for other factors associated with the constituting amino acids on the properties of aggregates resulting from the co-assembly of peptide sequences, specifically the phase separation of the sequences.

In this study, we employ a coarse-grained Molecular Dynamics

E-mail address: meenakshi.dutt@rutgers.edu (M. Dutt).

^{*} Corresponding author.

¹ Equal Contributions.

approach to studying a two component system consisting of V_6K_2 and V_6K_3 . Special attention is paid to the interaction energies of the system and their effect on the observed assembly characteristics. We set up and validate an appropriate model for the system and discuss the limitations of the approach. The validated model is then used to simulate the coassembly of V_6K_2 and V_6K_3 by varying their relative concentrations and studying their effect on the observable properties of the assemblies, specifically the phase separation of the two peptide sequences. The results from our study demonstrate the impact of difference in the polymerization of the charged amino acid on the properties of co-assemblies encompassing lipomimetic amphiphilic peptides. These results can potentially guide the development of novel peptide based materials, encompassing other similar peptide sequences, with multifunctional characteristics.

2. Materials and methods

2.1. Molecular dynamics simulations

Molecular Dynamics (MD) is a simulation technique that involves computing the motion of atoms and molecules. Atoms and molecules are represented as spheres that can interact with each other via a force field, and Newton's equations of motion are integrated over time to study the dynamics of the system. However, MD simulations can become prohibitively expensive when carried out at atomistic resolution. This is particularly true for systems that display aggregation behavior, a phenomenon that occurs over spatiotemporal scales spanning several hundreds of nanometers and several microseconds. To mitigate this cost, coarse graining is a popular technique employed in the study of selfassembling systems. We use the MARTINI coarse graining scheme, where four heavy (non-hydrogen) atoms are represented by a single bead. The MARTINI model encompasses simple analytical functional forms and maintains cross compatibility across a wide range of biomolecules such as polymers, lipids, peptides, and DNA [8]. All simulations are carried out using the GROMACS MD engine [9].

2.2. Peptide sequences

This study focuses on two specific oligopeptides: V_6K_2 and V_6K_3 . These peptides are eight and nine amino acids in length, respectively. These peptides have identical hydrophobic tails, and different hydrophilic heads, while composed of the same amino acid residues, the hydrophilic heads vary by one residue in length. This ensures that factors such as differences in hydrophilicity are controlled for, and only steric factors are at play. The peptide chains are almost identical with respect to sequence barring a single additional amino acid residue (i.e., Lysine) in the case of V_6K_3 . Therefore, the hydrophobic tails are identical. The hydrophilic heads are also composed of only Lysines in both cases, the only difference being length. This implies that on a per-residue basis, they are identical, and the only difference is the volume occupied by the two peptide types owing to the different lengths. Previous work [10] report the formation of nanofibers in pure systems of these peptide sequences.

Mixed peptide systems have been studied before: mixtures of FF and FNF systems display a rich polymorphism including nanotubes, vesicles and lamellae [7]. Another mixed peptide system encompassing FF and FFF on the other hand displays solid nanostructures without a water core, such as nanospheres and toroids [1c].

2.3. Coarse-graining and system parameterization

Each coarse-grained bead represents approximately four heavy (i.e. non-Hydrogen) atoms. The Valine residues are therefore represented by two beads each, and the Lysine residues are represented by three beads each, as shown in Fig. 1. The peptides are capped with acyl/N-Methylamine, i.e., the C and N termini of the peptides are assumed to

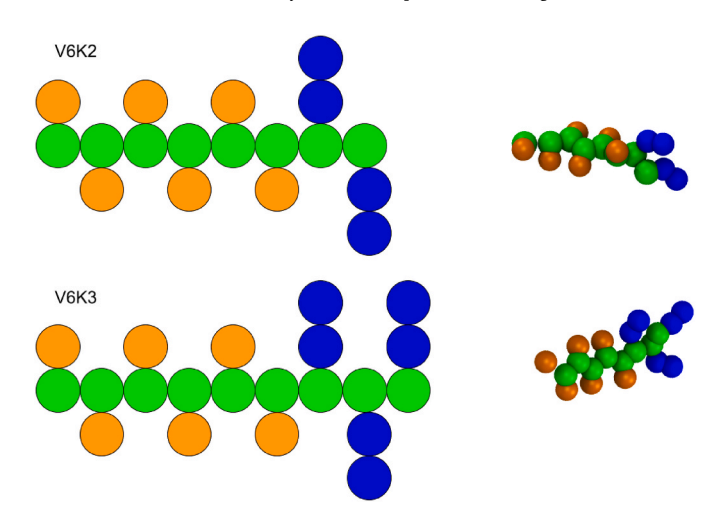


Fig. 1. (Left) coarse-grained representations of V_6K_2 and V_6K_3 peptides according to the MARTINI coarse-graining scheme. The green beads represent backbones, orange beads represent the Valine side chains and the blue beads represent the Lysine side chains. (Right) VMD rendition of the peptide sequences. (For interpretation of the references to colour in this figure legend, the reader is referred to the Web version of this article.)

not carry a charge. The side chains of the Lysine residues, however, carry a positive charge as described in an earlier study [8]. To ensure charge neutrality of the system, the boxes are also populated with the appropriate number of chloride counterions.

The MARTINI model requires the specification of a "bead type" parameter that varies based on the secondary structure of the peptide. For example, a helix structure, a random coil and a beta sheet structure for a peptide will change the bead type of a given residue based on the state of the peptide fragment the residue exists in. We assume that all structures are beta sheets: V₆ has been shown to exist predominantly in tightly packed beta sheet structures in an all atom replica exchange study [11]. While this study makes it clear that the V₆ chain does exhibit a small propensity to exist in other secondary structures, this assumption has been made for simplicity. Bond lengths are set to 0.35 nm between the backbone beads. The backbone-side chain bond of the Valine residue is defined as a distance constraint (via the LINCS algorithm) set to 0.265 nm. In the Lysine residue, the backbone-side chain bond and side chain-side chain bond are set to 0.33 nm and 0.28 nm respectively with a force constant of 5000 kJ/nm^2/mol. In keeping with the beta sheet secondary structure, the extended conformation was used to describe the torsions, i.e., all torsion angles were set to 180° with a force constant of 10 kJ/mol. A Parrinello-Rahman barostat is employed to maintain the pressure at 1 bar. The temperature is maintained at 310 K using a velocity rescaling thermostat. Since pure velocity rescaling cannot rigorously reproduce configurations associated with the canonical ensemble, a stochastic term is added to the thermostat as described by Bussi [12]. All simulations were first energy-minimized using the steepest descent integrator until the maximum force between any two given particles was less than a threshold of 10 nN, followed by equilibration for 1 ns using a timestep of 5 fs? The simulations were then run for 2 µs with a timestep

Both the polarizable [14] as well as non-polarizable, or standard MARTINI [15], water models were employed. The two approaches to modeling of water were employed to account for differences in behavior arising due to the presence of charged groups in the system. It must be noted that the peptide model was also changed to the corresponding polarizable (MARTINI v2.2P) or non-polarizable (v2.2) models.

The standard water model does not carry any charges, and therefore remains entirely unaffected by electrostatic and polarization effects, the energetic discrepancies arising from which are accounted for implicitly using a uniform dielectric constant [14]. This assumption can reproduce

the properties of bulk water, but in modeling the behavior of water at interfaces, interaction strengths of polar substances are often underestimated due to the significant contribution from electrostatic interactions. The polarizable MARTINI water model accounts for this by representing water by three beads. Two of the beads carry opposite charges flanking one central neutral bead. This is in contrast to the standard water model which uses a single neutral bead to represent four water molecules.

The polarizable model yielded fibers as shown in Fig. 2a. These fibers were somewhat amorphous, but displayed aspect ratios large enough to interact across the periodic boundary and yield a continuous fiber-like structure. It must be noted that this fiber, as seen in the figure, did not display an uniform diameter.

The non-polarizable model, in contrast, yielded nanofiber structures with a near uniform diameter along their length through the simulation box, as shown in Fig. 2b. As a cursory metric to compare the emergent physical properties of the fibers in the two models, we chose the solvent accessible surface area (SASA). Table 1 shows the SASA as well as contributions of the Coulombic and Lennard Jones (LJ) components of the interactions between particles in the polarizable as well as non-polarizable systems. We observe that the SASA values are within a 3% error of each other. Interaction energies are however different: we observe the dominance of the LJ component in the driving forces in the non-polarizable systems. The reduction in strengths of the water-peptide interactions due to the non-polarizable nature of the water model exaggerates the hydrophobic effect driving the peptides to aggregate.

Table 1: Comparison between the Solvent Accessible Surface Areas (SASA) as well as Lennard Jones (LJ) and Coulombic components of interactions in polarizable and non-polarizable systems. SASA values for the two systems are within a 3% error of each other. Interaction energies display a significant difference: In the non-polarizable case, the driving forces behind aggregation are dominated by the LJ component, highlighting the lipomimetic nature of the system.

The non-polarizable model also displayed a significant computational advantage. The polarizable model for this specific set of systems required a shorter timestep of 5 fs to run stably, in addition to an increased cost-per-timestep due to a larger particle count owing to the 3-particle representation of the solvent. Ultimately, the non-polarizable model resulted in approximately a $\sim\!2.5\mathrm{X}$ speedup over the polarizable model on the ACCESS TACC Stampede 2 supercomputer on one full node.

Therefore, it was determined that the non-polarizable water model was not only computationally more efficient, but also yielded results that agreed better with prior experimental [10b] studies, i.e., fibrillar structures of similar diameter. This model is therefore employed to study mixed systems, and we make clear that these results must be interpreted with the above in mind. The outcomes of these simulations are discussed

in the next section.

Simulations of larger systems were set up with 650 V_6K_2 peptides in a 17 nm \times 17 nm x 17 nm simulation box using the non-polarizable water model for validation, and to rule out finite size effects on the structural stability of the self-assembled fibers observed. These simulations yielded larger, more flexible nanofibers than those observed in the smaller simulation boxes. We attribute the increase in flexibility to the larger size of the simulation boxes that not only allow for more spatial configurations of the fiber, i.e., a larger box volume leading to greater freedom for the fiber to bend and coil around before needing to pass through a periodic wall, but also the mechanics of the fiber operating closer to its persistence length. Ten independent trajectories were generated with this setup for statistical significance and these fibers were observed in nine of them. One such fiber is shown Fig. 3.

3. Results and discussion

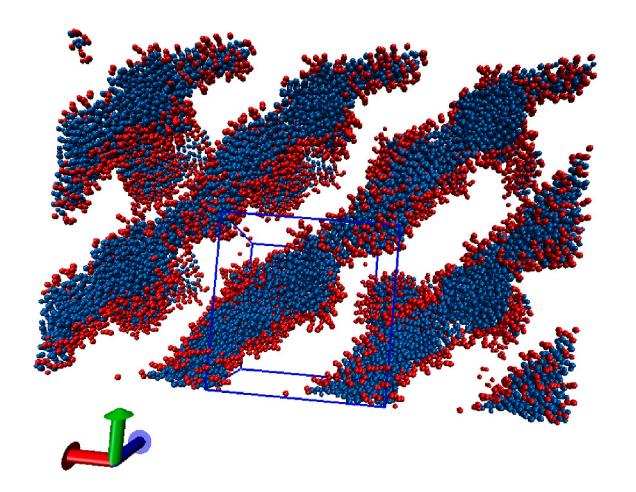
We set up simulations of mixed systems in order to generate a phase space of self-assembled morphologies while varying the relative concentrations of two peptide sequences: V_6K_2 and V_6K_3 . These peptides were chosen for their identical hydrophobic tails, whereas the hydrophilic heads are identical in all aspects except length. V_6K_3 has a three-Lysine head as opposed to two. The overall concentration of peptides was kept constant (650 peptides in a 17x17x17 cubic nm simulation box ~ 0.132 peptides/cubic nm) and the relative concentration of the two was varied from 0% V_6K_2 (pure V_6K_3) to 100% V_6K_2 . Ten independent trajectories were generated for all systems for statistical significance. Systems were set up identically to the pure systems discussed in the prior section.

3.1. Radius of gyration of polar head group

The Radius of Gyration (RoG) is a fundamentally important metric in biomolecular systems. It provides insight into the approximate "effective volume" occupied by a given species and hence, is an important tool for studying steric effects in a chemical system. The RoG of the polar head beads was computed using the native gmx gyrate tool in GROMACS. We find the RoG of both species remains independent of relative concentration, with V_6K_3 demonstrating a $\sim 17\%$ larger RoG owing to the larger head group. This is shown in Fig. 4. This result is significant, since it has a bearing on other system properties that are discussed in the forthcoming sections.

3.2. Solvent accessible surface area

The SASA was computed for all systems using the *gmx sasa* tool native to GROMACS. SASA is computed by measuring the total surface



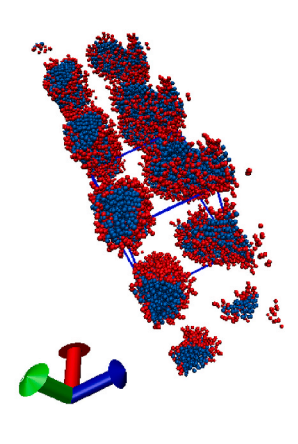
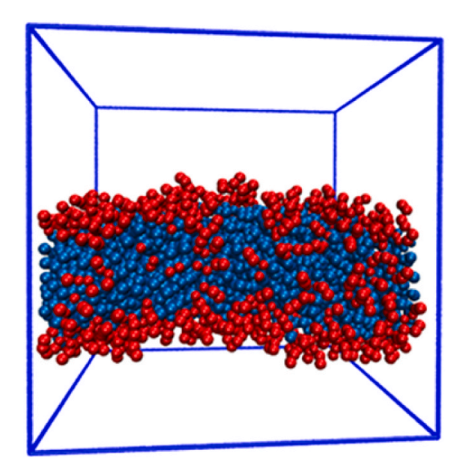


Fig. 2a. Polarizable water model was used for simulating the aggregation of 200 V_6K_2 peptides in a 11 nm \times 11 nm \times 11 nm simulation box. The simulation yielded nanofibers. However, the fibers were not consistent in diameter. The system was imaged by zooming out using periodic boundary conditions to demonstrate fiber formation with inconsistent diameter (left: side view, right: axial view). The periodic box is also shown. Color scheme: red beads (Lysine) and blue beads (Valine), axes: X (red), Y(green), Z (blue). (For interpretation of the references to colour in this figure legend, the reader is referred to the Web version of this article.)



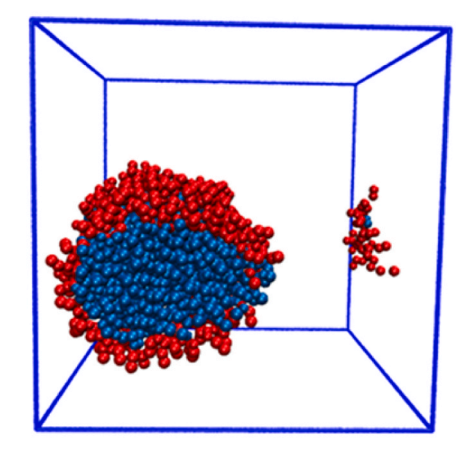


Fig. 2b. Non-polarizable water model was used for simulating the aggregation of $200 \text{ V}_6\text{K}_2$ peptides in a $11 \text{ nm} \times 11 \text{ nm} \times 11 \text{ nm}$ simulation box. The system yielded nanofibers with solid cores and constant diameter across the length (left: side view, right: axial view). Color scheme: red beads (Lysine) and blue beads (Valine). (For interpretation of the references to colour in this figure legend, the reader is referred to the Web version of this article.)

Table 1
SASA, van der Waals interactions and Coulombic interactions for Polarizable and Non Polarizable systems.

System	SASA (sq. nm)	Potential Energy (LJ Component, mean, kJ/ mol)	Potential Energy (Coulombic Component, mean, kJ/mol)
Polarizable	995.347	-269019	-156877
Nonpolarizable	964.974	-371035	-2436

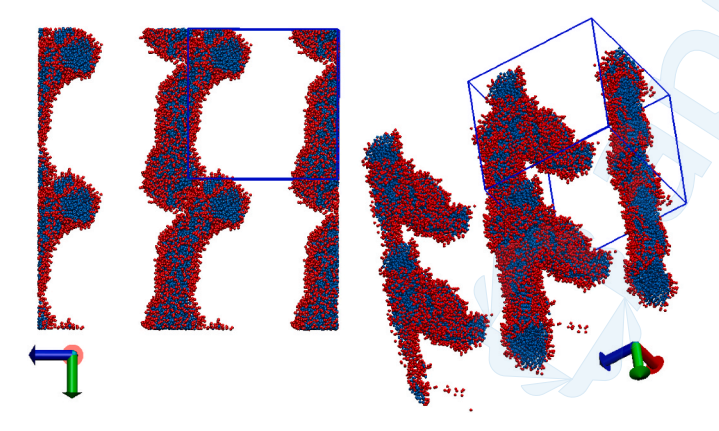


Fig. 3. 650 V_6K_2 peptides in a 17 nm \times 17 nm \times 17 nm simulation box seen from two different angles. Fibers observed here are more flexible and branching compared to the smaller systems. The system was imaged by zooming out using periodic boundary conditions to demonstrate fiber formation with consistent diameter. Left: dead-on view along X-Axis, Right: inverted isometric view to show fiber flexion and branching structure. Color scheme: red (Lysine) and blue (Valine), axes: X (red), Y(green), Z(blue). (For interpretation of the references to colour in this figure legend, the reader is referred to the Web version of this article.)

area across all peptides in the simulation box that are interacting with at least one solvent particle. The observed SASA for each system is shown in Fig. 5. The SASA decreases as the concentration of V_6K_2 increases. This is due to the fact that the smaller head group of V_6K_2 reduces the area per molecule and hence the surface area. This is also in line with the radius of gyration measurement reported: larger abundance of V_6K_2 , i.e., the peptide with the smaller RoG, causes the SASA to drop proportionally.

3.3. Cluster analysis

Cluster analysis was performed by counting the number of clusters of each peptide type in the simulation box. For the purpose of a rigorous definition of the term "cluster", we use the average RoG for the Lysine head groups of each system. These are observed at 0.376 nm and 0.452 nm for the V₆K₂ and V₆K₃ systems, respectively. This distance is considered to be the maximum interaction distance between two head groups that are part of the same cluster (not to be confused with the minimum possible separation between two head groups). Essentially, if a given head group i is outside the range of the first exclusion shell of any head group j in a given cluster, that head group i is not considered to be a part of that cluster. Therefore, if there are N peptides/head groups in the box, all separated by distances greater than the first exclusion shell, they are counted as N separate clusters. We find, through this approach, that the number of clusters of each species hits a maximum at 20% relative concentration of that specific species: rising sharply until the 20% relative concentration is reached and then gradually decreasing. This is shown in Fig. 7. This observation implies that at lower concentrations, the species is spatially well spread out across the simulation box. As the concentrations rise to \sim 20%, the number of peptides of the species in question increase but do not aggregate, leading to a large cluster count. As the relative concentration further increases, peptides come within proximity of each other and aggregate, causing the cluster count to gradually decrease. An interesting feature of this system is that at exactly 50% relative concentration (i.e., there is exactly the same number of both species in the system), the V₆K₃ component has far fewer clusters. It must also be noted that V₆K₃ peptides have a lower maximum cluster count than V₆K₂. We attribute this to the greater radius of gyration of the K₃-head group, leading to a larger excluded volume which allows for each V₆K₃ head group having a greater "reach", causing them to register as part of the same cluster. It must be clarified that clustering here does not imply "preferential" interaction between two V₆K₃ peptides: the larger head groups are hydrophilic, and therefore do not explicitly "attract" each other. It merely implies that the larger head group excluded volume leads to more peptides being "detected" to be within the interaction shell of a given reference peptide. The greater clustering behavior of V₆K₃ due to its greater detection radius is seen in Figs. 6–8. It must be pointed out here that the clusters reported are not strictly "aggregates", but an extended percolating network.

Cluster sizes also show some interesting trends. Fig. 7 shows cluster size (i.e., number of peptides in a single cluster) as a function of the species concentration. Between the 30%–60% relative species concentrations, the two species show large gaps in cluster sizes. Individual clusters are smaller on average for the smaller species. This is attributed

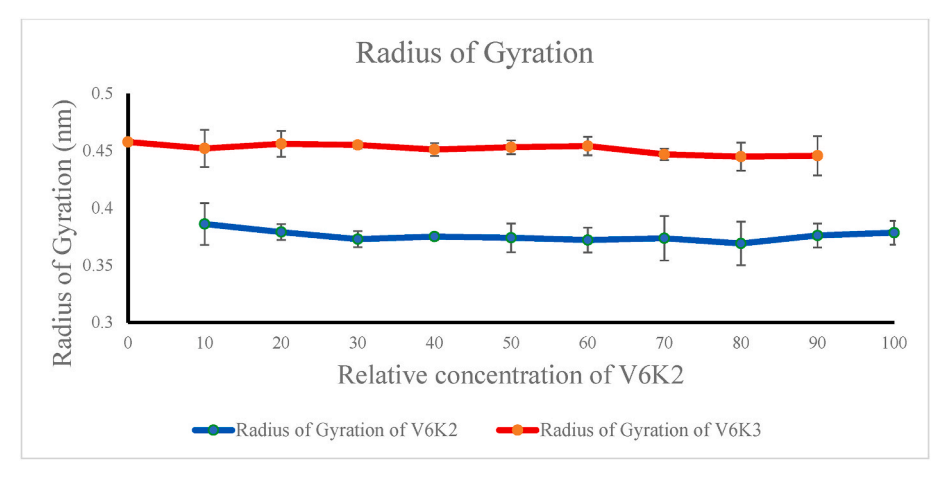
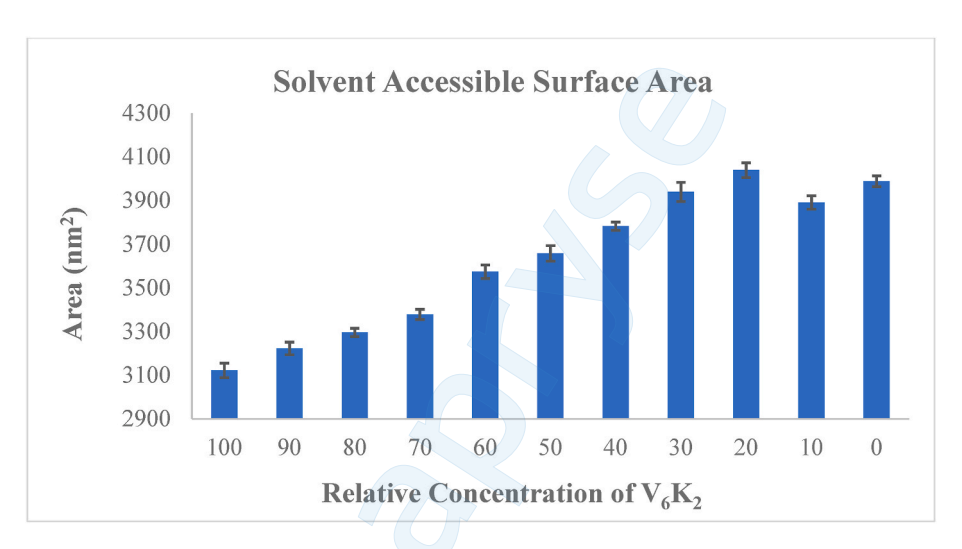


Fig. 4. Radius of Gyration (RoG) centered on the center of mass of the hydrophilic head group, plotted as a function of relative concentration of V₆K₂.



 $\textbf{Fig. 5.} \ \ \text{Solvent accessible surface area (Area) plotted as a function of relative concentration of V_6K_2. The SASA increases with decreasing concentration of V_6K_2.}$

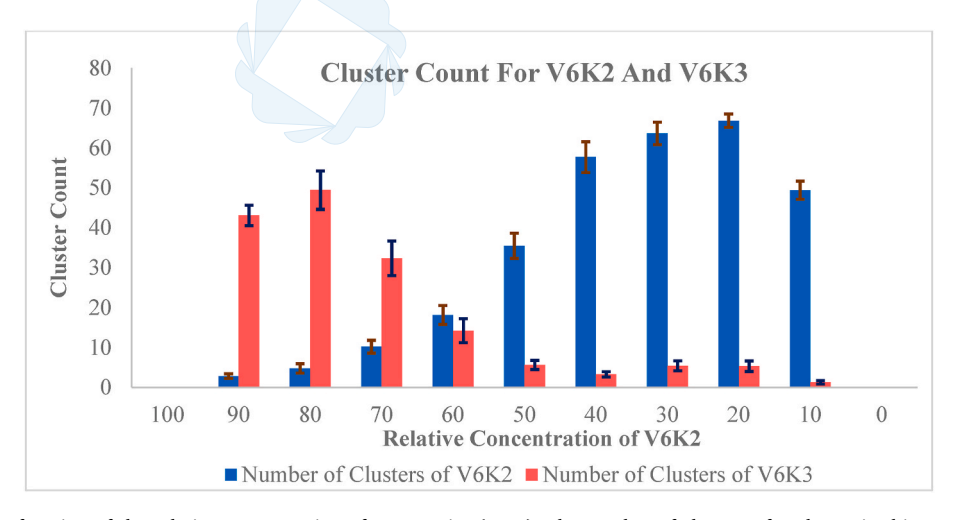


Fig. 6. Cluster count as a function of the relative concentration of one species (V_6K_2) . The number of clusters of each species hits a maximum at 20% relative concentration of that specific species, rising sharply until the 20% relative concentration is reached and then gradually decreases.

to the larger "reach" of the V_6K_3 species that causes a larger number of peptides to be counted as part of a given cluster.

3.4. Association energies

Calculations of the energies are necessary to understand the nature of the interactions between the various species in the system. These

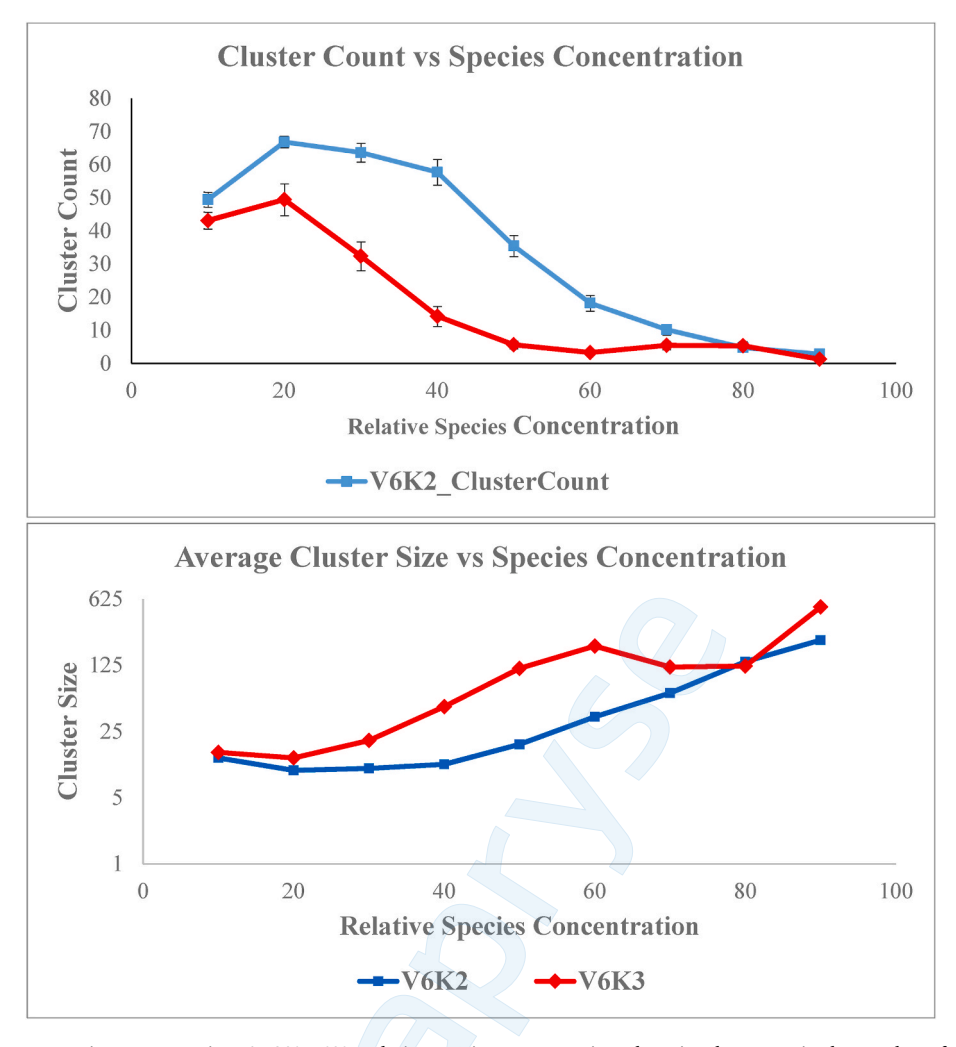


Fig. 7. (Top) Cluster count vs species concentration. At 30%-60% relative species concentration, there is a large gap in the number of clusters observed for each species at the same relative concentration. (Bottom) Average cluster size (computed as total number of peptides, i.e. 650, divided by Cluster Count), log scale. Individual clusters on average are smaller for the V_6K_2 species.

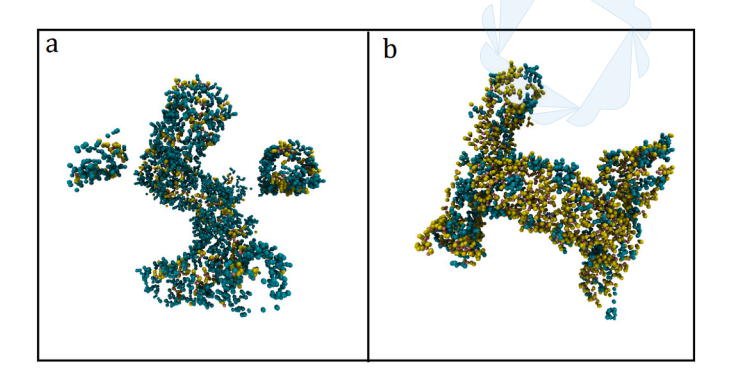


Fig. 8. Self-assembled nanostructures for mixtures encompassing (a) 30% V_6K_2 , and (b) 70% V_6K_2 . Both systems consist of 650 peptides. Figures show a visual representation of the degree of dispersion of the minor phases. Only the Lysine head groups are shown for visual clarity (Orange: backbones, green: K2, teal: K3). A small degree of self-association is observed for the V_6K_2 species in (a) due to the low concentration (63 clusters), whereas in (b) the V_6K_3 species demonstrates a significantly larger degree of self-association despite the low concentration (32 clusters). (For interpretation of the references to colour in this figure legend, the reader is referred to the Web version of this article.)

calculations elucidate the dominant forms of interaction in the system and help identify the factors responsible for the observed phenomena. The energies were computed using the native GROMACS tool gmx energy. We computed energies between both like and unlike species, and also decomposed the energies into their respective LJ and Coulombic components. Figs. 9 and 10 shows the interaction energies between the like and unlike species. The energies are large negative values, suggesting that the LJ component dominates. To verify this, we decomposed the energies into their LJ and Coulombic components. We find that the LJ components are an order of magnitude greater than the Coulombic components. This decomposition is shown in Fig. 10. It must be noted that this is likely an underestimation of the Coulombic component as a result of the non-polarizable model, and the results must therefore be interpreted with care. Further, the energies show monotonic trends as a function of the relative concentration of the species. This is in line with our intuition and expectation: the lower concentration of a given species is associated with a less negative self-interaction energy for that species. This is due to the fact that as the concentration of a specific species reduces, there are fewer energetic contributors to the overall energy. Therefore, as the fraction of species "B" increases, U_AA becomes more positive, due to a reduction of species A, and vice versa. The per-peptide energies also show the same trend: this is due to the fact that each peptide interacting with its neighbors has fewer like peptides to interact with as the proportion of the unlike peptide species increases.

Interspecies interaction energies (Fig. 11) show non-monotonic

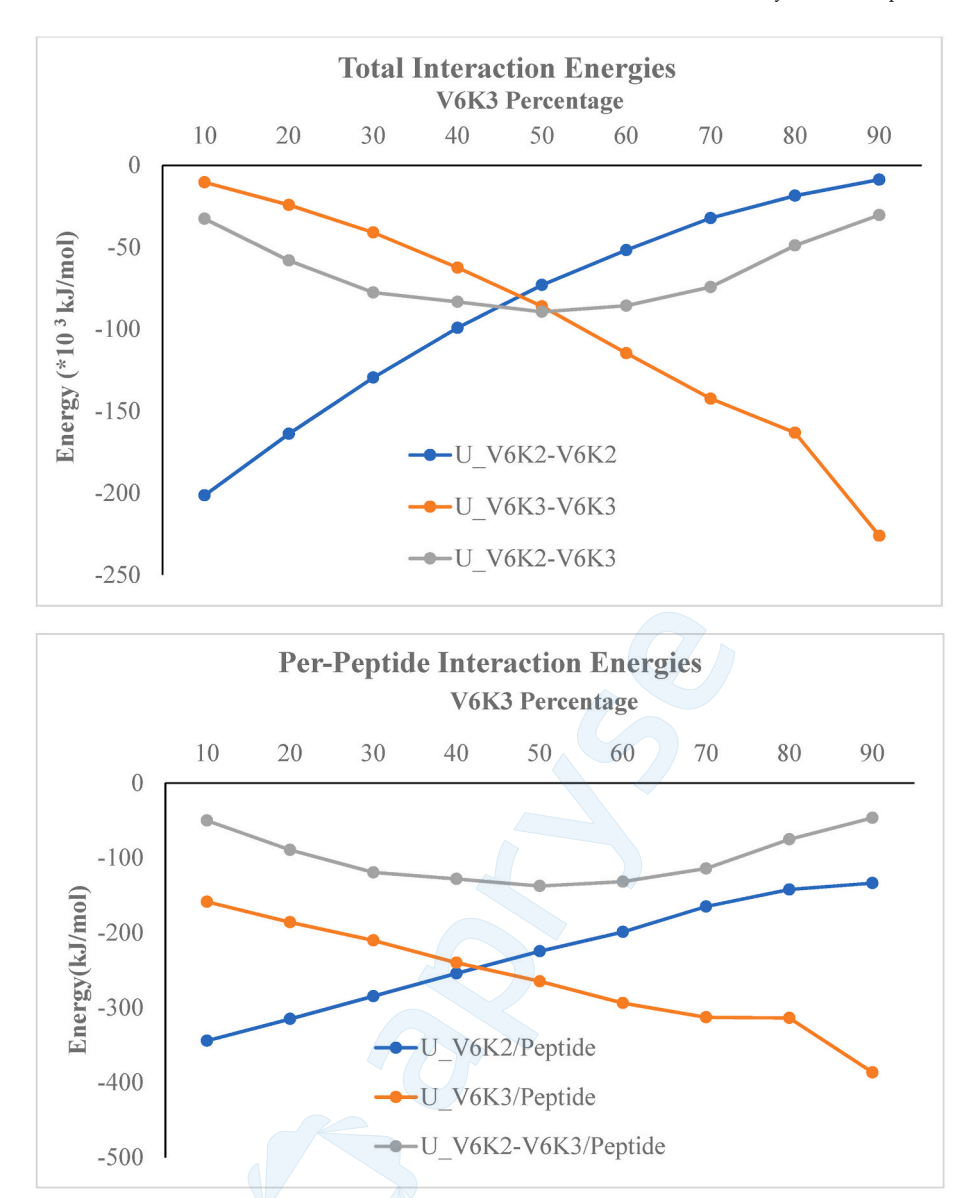


Fig. 9. (Top) Association energies vs fraction of V_6K_3 . As the fraction of species V_6K_3 increases, U_V6K2_V6K2 becomes more positive, and vice versa. (Bottom) Perpetide energies (computed as Association Energy divided by total number of peptides, i.e. 650) show the same trends.

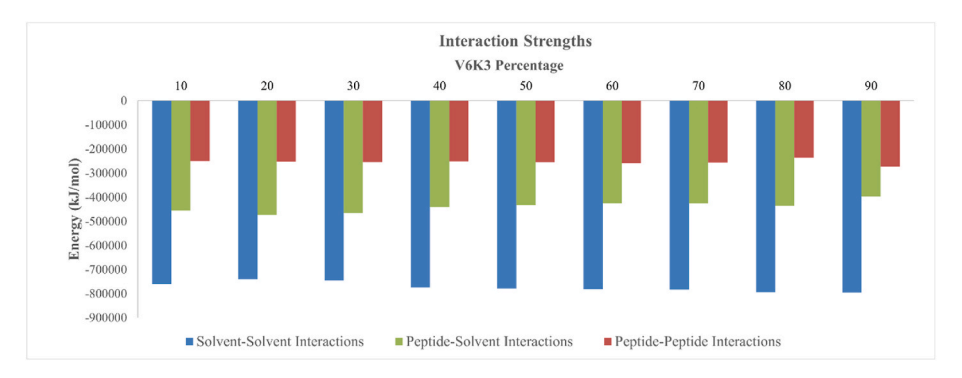


Fig. 10. Relative interaction strengths of various molecules in the system. The large negative value of solvent-solvent interactions in relation to other types of interactions is in line with our expectations for a system driven by the hydrophobic effect.

behavior with changing concentration of each species. The Coulombic repulsive component and LJ attractive component peak at about 50%. Further, this decomposition in the interaction confirms that the hydrophobic effect dominates all interactions in these systems, i.e., the

aggregation is driven by preferential LJ interactions between peptides. This is in line with our expectation for a lipomimetic system.

An interesting point to note here is that at exactly 50% (325 V_6K_2 peptides and 325 V_6K_3 peptides), the V_6K_2 like species interaction is

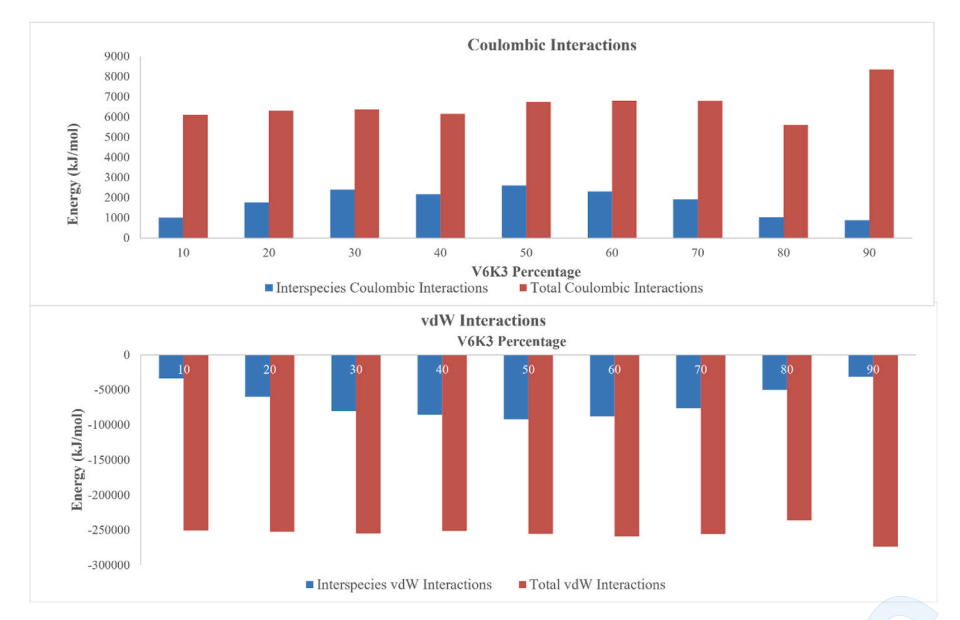


Fig. 11. Total and interspecies LJ and Coulombic decomposition. LJ component dominates, and the interspecies component of the LJ and Coulombic interactions show non-monotonic behavior with changing relative concentration. Interspecies Coulombic force is non-monotonically repulsive and is an order of magnitude smaller than the attractive LJ component. The total energies remain roughly constant. This is attributed to the fact that each system has the same number of peptides interacting with each other.

higher than the corresponding quantity for V_6K_3 . This suggests that the larger molecule has a slightly greater propensity to self-associate. We attribute this behavior to the presence of an additional Lysine residue adding to the dominant attractive LJ forces that exist between two given V_6K_3 peptides: while the two Lysine groups are hydrophilic and preferentially attract the solvent particles, the forces between them are not explicitly repulsive: the forces between any two given lysine residues are weakly attractive as defined in the MARTINI force field.

This effect combined with the stabilization of repulsion between like charges as a result of salt bridging between the Lysine groups by Cl-counterions prevents the disruption of local structure explains the observed behavior (shown in Fig. 12). The interaction between two Lysines is repulsive due to like charges. However, the overall LJ interactions are still overwhelmingly attractive. The Cl- ions therefore provide additional stabilization to local structures that would otherwise be disrupted due to their proximity.

3.5. Degree of association

The degree of association is a metric of interspecies interactions computed using the global interaction cutoff. The total number of species within the interaction cutoff (i.e., 1.2 nm, the MARTINI force field global cutoff) are counted from each reference particle and normalized

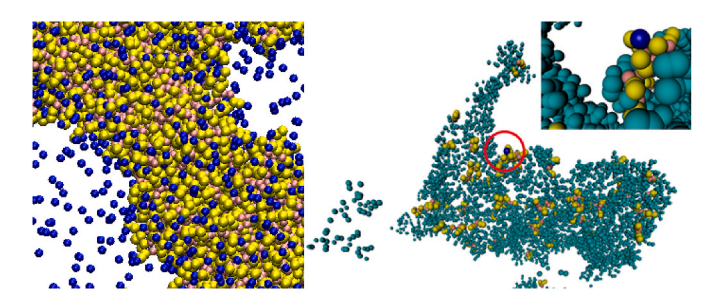


Fig. 12. (Left) Chloride counterions shown in a full simulation box. (Right) Local stabilization by counterion salt bridge formation. For clarity, only surface Lysine residues are shown. Grey beads represent the Lysines belonging to V_6K_2 , green beads represent Lysines belonging to V_6K_3 , and the dark blue bead is a single counterion stabilizing multiple Lysine residues via salt bridging. Only a single counterion is shown for clarity (encircled and zoomed in the inset). (For interpretation of the references to colour in this figure legend, the reader is referred to the Web version of this article.)

by the total number of peptides (i.e. 650). This property is plotted in Fig. 13. The greatest degree of association between unlike species is observed at $\sim\!50\%$ ratio. This is due to the fact that roughly equal concentrations of each species maximize the probability of occurrence of interspecies interactions. This explains the behavior of the interspecies interaction energy as shown in Fig. 11, which reaches its most negative value at the 50% V_6K_2 mark.

The self-assembled nanostructures demonstrate varying degrees of clustering across varying relative concentrations as shown in Fig. 14. The overall morphology of the self-assembled structures does not appear to change significantly with relative concentrations. In all cases, fibrillar aggregates are observed. Differences are observed not in the overall morphology, but in the behavior of the surface head groups of the two peptides and the degrees of interactions for like-species and unlike-species. These differences are summarized as follows: the larger spatial occupancy of the 3-Lysine head groups causes a larger SASA as the proportion of the larger peptide increases. Further, the larger interaction range of the bigger head group causes larger "networks" of head groups to be detected as the V_6K_3 concentration increases relative to the V_6K_2 concentration.

4. Conclusions

In this study, we examine the co-assembly of lipomimetic aliphatic peptides via coarse-grained MD simulations. The peptide sequences are selected such that the hydrophobic and polar amino acid residues are identical along with the polymerization of the hydrophobic amino acid. The two sequences differ in the polymerization of the polar amino acid residue. Hence, the study examined the effects of incremental differences in polymerization on the properties of aggregates resulting from the co-assembly of peptides while controlling for other factors associated with the constituting amino acids. Specifically, we were interested in investigating the phase separation of the two peptide sequences in the aggregates.

The peptide models were first generated and validated individually, and then evaluated for co-assembly. We have tested both the polarizable and non-polarizable MARTINI models, and find that the non-polarizable model yields results closer to experiments and also provides a factor of 2.5 speedup in computation time. While the non-polarizable model yields a much lower overall Coulombic component, the polarizable model still shows a $\sim\!71\%$ higher estimate for the LJ component. Our system consists of two components that are highly similar, with the

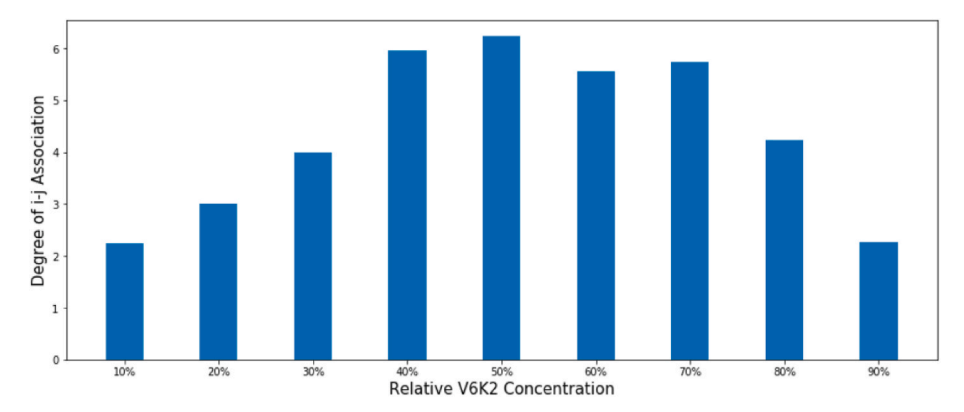


Fig. 13. i-j Interactions (i.e., LJ cutoff) plotted as the degree of association.

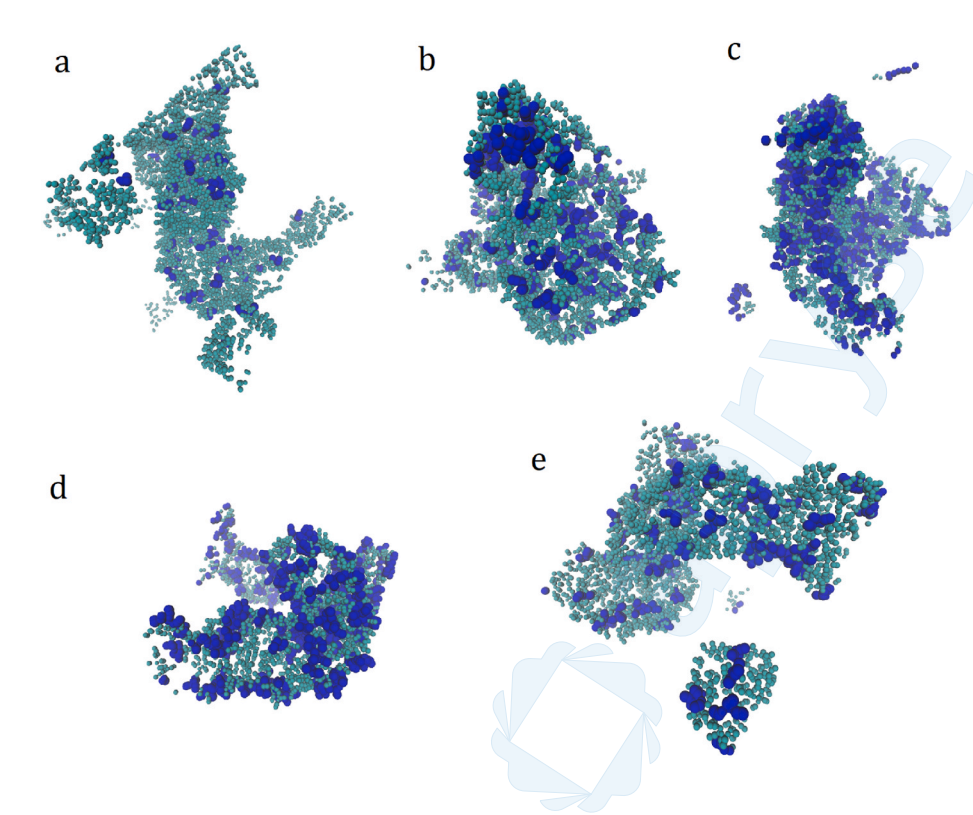


Fig. 14. Self-assembled nanostructures showing species self-association across varying relative concentrations of V_6K_2 . Only surface Lysines are shown for clarity. The minor component is highlighted in deep blue. (a) 10%, (b) 30%, (c) 50% (in this case, V_6K_2 is highlighted in dark blue), (d) 70%, and (e) 90% V_6K_2 . V_6K_3 shows greater self-association across the simulation space. (For interpretation of the references to colour in this figure legend, the reader is referred to the Web version of this article.)

exception of V_6K_3 having one additional Lysine amino acid. We observe that the interactions of the two species are dominated by the hydrophobic effect. The phenomenon of phase segregation is observed, and seems to be driven by the preferential self-association of the V_6K_3 peptides.

The V_6K_3 sequence displays a greater propensity to self-associate as a combined result of the larger volume of the peptide as shown by the radius of gyration, leading to greater range of interactions between two V_6K_3 peptides. The stabilization of like-charge Lysine groups through the formation of Chloride salt bridges is observed. It must be stressed that "self-association" here simply refers to the fact that the increased interaction range between V_6K_3 peptides allows for the detection of larger clusters. The Chloride salt bridges provide local stabilization by preventing disruption of the packing by like-charge repulsion between the head groups.

Our study demonstrates how properties of co-assemblies encompassing lipomimetic amphiphilic peptides are affected by the difference in the polymerization of the charged amino acid. The results from this study can potentially inspire the development of new peptide based materials, encompassing analogous peptide sequences, with novel

multifunctional characteristics. This work studies the effects of differing head group sizes on overall assembly properties. We have found that the larger head group of the V_6K_3 molecules results in a greater spatial "spread" for those molecules. Therefore, properties such as radius of gyration, SASA and interaction range are significantly affected. Larger head groups than a 3-Lysine (such as 4-, 5- or 6-Lysine) are expected to show similar behavior, but further studies with all atom and coarse grained simulations are necessary to confirm this.

Declaration of competing interest

The authors declare the following financial interests/personal relationships which may be considered as potential competing interests: Meenakshi Dutt reports financial support was provided by National Science Foundation.

Data availability

Data will be made available on request.

Acknowledgements

S.M. acknowledges the Rutgers University Chemical and Biochemical Engineering Department for financial support. K.S. acknowledges the New Jersey Space Grant Consortium (NJSGC) (grant number NNX15AK05H). M.D. gratefully acknowledges NSF CAREER award DMR-1654325. All authors gratefully acknowledge the use of computational resources supported by NSF ACCESS (allocation DMR-140125).

References

- [1] (a) S. Mushnoori, C.Y. Lu, K. Schmidt, E. Zang, M. Dutt, Peptide-based vesicles and droplets: a review, J. Phys. Condens. Matter (2020);
 - (b) E. Gazit, A possible role for pi-stacking in the self-assembly of amyloid fibrils, Faseb. J. 16 (1) (2002) 77–83;
 - (c) C. Guo, Z.A. Amon, R.X. Qi, Q.W. Zhang, L. Adler-Abramovich, E. Gazit, G. H. Wei, Expanding the nanoarchitectural diversity through aromatic di- and tripeptide coassembly: nanostructures and molecular mechanisms, ACS Nano 10 (9) (2016) 8316–8324.
- [2] (a) D.G. Fatouros, D.A. Lamprou, A.J. Urquhart, S.N. Yannopoulos, I. S. Vizirianakis, S. Zhang, S. Koutsopoulos, Lipid-like self-assembling peptide nanovesicles for drug delivery, ACS Appl. Mater. Interfaces 6 (11) (2014) 8184–8189:
 - (b) S. Vauthey, S. Santoso, H. Gong, N. Watson, S. Zhang, Molecular self-assembly of surfactant-like peptides to form nanotubes and nanovesicles, Proc. Natl. Acad. Sci. U. S. A. 99 (8) (2002) 5355–5360;
 - (c) N. Thota, J. Jiang, Self-assembly of amphiphilic peptide (AF)6H5K15 derivatives: roles of hydrophilic and hydrophobic residues, J. Phys. Chem. B 118 (10) (2014) 2683–2692:
 - (d) N. Thota, Z. Luo, Z. Hu, J. Jiang, Self-assembly of amphiphilic peptide (AF) 6H5K15: coarse-grained molecular dynamics simulation, J. Phys. Chem. B 117 (33) (2013) 9690–9698.
- [3] R.J. Swanekamp, J.T. DiMaio, C.J. Bowerman, B.L. Nilsson, Coassembly of enantiomeric amphipathic peptides into amyloid-inspired rippled beta-sheet fibrils, J. Am. Chem. Soc. 134 (12) (2012) 5556–5559.
- [4] K. Nagy-Smith, P.J. Beltramo, E. Moore, R. Tycko, E.M. Furst, J.P. Schneider, Molecular, local, and network-level basis for the enhanced stiffness of hydrogel networks formed from coassembled racemic peptides: predictions from pauling and corey, ACS Cent. Sci. 3 (6) (2017) 586–597.
- [5] Z. Yu, A. Erbas, F. Tantakitti, L.C. Palmer, J.A. Jackman, M. Olvera de la Cruz, N. J. Cho, S.I. Stupp, Co-Assembly of peptide amphiphiles and lipids into

- supramolecular nanostructures driven by anion-pi interactions, J. Am. Chem. Soc. 139 (23) (2017) 7823–7830.
- [6] (a) P. Makam, E. Gazit, Minimalistic peptide supramolecular co-assembly: expanding the conformational space for nanotechnology, Chem. Soc. Rev. 47 (10) (2018) 3406–3420;
 - (b) D.M. Raymond, B.L. Nilsson, Multicomponent peptide assemblies, Chem. Soc. Rev. 47 (10) (2018) 3659–3720.
- [7] S. Mushnoori, K. Schmidt, V. Nanda, M. Dutt, Designing phenylalanine-based hybrid biological materials: controlling morphology via molecular composition, Org. Biomol. Chem. 16 (14) (2018) 2499–2507.
- [8] L. Monticelli, S.K. Kandasamy, X. Periole, R.G. Larson, D.P. Tieleman, S.J. Marrink, The MARTINI coarse-grained force field: extension to proteins, J. Chem. Theor. Comput. 4 (5) (2008) 819–834.
- [9] (a) B. Hess, C. Kutzner, D. van der Spoel, E. Lindahl, Gromacs 4: algorithms for highly efficient, load-balanced, and scalable molecular simulation, J. Chem. Theor. Comput. 4 (3) (2008) 435–447;
 - (b) S. Pall, A. Zhmurov, P. Bauer, M. Abraham, M. Lundborg, A. Gray, B. Hess, E. Lindahl, Heterogeneous parallelization and acceleration of molecular dynamics simulations in GROMACS, J. Chem. Phys. 153 (13) (2020), 134110,
 - (c) S. Pronk, S. Pall, R. Schulz, P. Larsson, P. Bjelkmar, R. Apostolov, M.R. Shirts, J.C. Smith, P.M. Kasson, D. van der Spoel, B. Hess, E. Lindahl, Gromacs 4.5: a high-throughput and highly parallel open source molecular simulation toolkit, Bioinformatics 29 (7) (2013) 845–854.
 - (d) D. Van Der Spoel, E. Lindahl, B. Hess, G. Groenhof, A.E. Mark, H.J. Berendsen, GROMACS: fast, flexible, and free, J. Comput. Chem. 26 (16) (2005) 1701–1718.
- [10] (a) N. Habibi, N. Kamaly, A. Memic, H. Shafiee, Self-assembled peptide-based nanostructures: smart nanomaterials toward targeted drug delivery, Nano Today 11 (1) (2016) 41–60;
 - (b) Q. Meng, Y. Kou, X. Ma, Y. Liang, L. Guo, C. Ni, K. Liu, Tunable self-assembled peptide amphiphile nanostructures, Langmuir 28 (11) (2012) 5017–5022.
- [11] Y. Sun, Z. Qian, C. Guo, G. Wei, Amphiphilic peptides A6K and V6K display distinct oligomeric structures and self-assembly dynamics: a combined all-atom and coarsegrained simulation study, Biomacromolecules 16 (9) (2015) 2940–2949.
- [12] G. Bussi, D. Donadio, M. Parrinello, Canonical sampling through velocity rescaling, J. Chem. Phys. 126 (1) (2007), 014101.
- [13] M.D. Xiang Yu, Implementation of dynamic coupling in hybrid Molecular Dynamics-Lattice Boltzmann approach: modeling aggregation of amphiphiles, Comput. Phys. Commun. 257 (2020). December.
- [14] S.O. Yesylevskyy, L.V. Schafer, D. Sengupta, S.J. Marrink, Polarizable water model for the coarse-grained MARTINI force field, PLoS Comput. Biol. 6 (6) (2010), e1000810.
- [15] D.H. de Jong, G. Singh, W.F. Bennett, C. Arnarez, T.A. Wassenaar, L.V. Schafer, X. Periole, D.P. Tieleman, S.J. Marrink, Improved parameters for the martini coarse-grained protein force field, J. Chem. Theor. Comput. 9 (1) (2013) 687–697.